Fluorescence Analysis of a Dynamic Loop in the PCAF/GCN5 Histone Acetyltransferase†

Yujun Zheng,‡ Fatemah Mamdani,‡ Dimitri Toptygin,§ Ludwig Brand,§ James T. Stivers,‡ and Philip A. Cole*,‡

Department of Pharmacology and Molecular Sciences, Johns Hopkins University School of Medicine, Baltimore, Maryland 21205, and Department of Biology, Johns Hopkins University, Baltimore, Maryland 21218

Received April 27, 2005; Revised Manuscript Received June 13, 2005

ABSTRACT: PCAF and GCN5 are histone acetyltransferase (HAT) paralogs which play roles in the remodeling of chromatin in health and disease. Previously, a conformationally flexible loop in the catalytic domain had been observed in the X-ray structures of GCN5 in different liganded states. Here, the conformation and dynamics of this PCAF/GCN5 α5−β6 loop was investigated in solution using tryptophan fluorescence. A mutant human PCAF HAT domain ($PCAF^{Wloop}$) was created in which the natural tryptophan (Trp-514) remote from the α5−β6 loop was replaced with tyrosine and a glutamate within the loop (Glu-641) was substituted with tryptophan. This $PCAF^{Wloop}$ protein exhibited catalytic parameters within 3-fold of those of the wild-type PCAF catalytic domain, suggesting that the loop mutation was not deleterious for HAT activity. While saturating CoASH induced a 30% quenching of Trp fluorescence in $PCAF^{Wloop}$, binding of the high-affinity bisubstrate analogue H3-CoA-20 led to a 2-fold fluorescence increase. These different effects correlate with the different α5−β6 loop conformations seen previously in X-ray structures. On the basis of stopped-flow fluorescence studies, binding of H3-CoA-20 to $PCAF^{Wloop}$ proceeds via a rapid association step followed by a slower conformational change involving loop movement. Time-resolved fluorescence measurements support a model in which the α5−β6 loop in the H3-CoA-20−$PCAF^{Wloop}$ complex exists in a narrower ensemble of conformations compared to free $PCAF^{Wloop}$. The relevance of loop dynamics to PCAF/GCN5 catalysis and substrate specificity are discussed.

The histone acetyltransferases (HATs) are critical enzymes in the regulation of chromatin structure and gene expression (*1*−*3*). The first nuclear HAT to be discovered, GCN5,[1] and its paralog, PCAF, are conserved in organisms from yeast to humans, and PCAF and GCN5 have served as paradigms for the biochemical analysis of HAT structure, mechanism, and function (*1*−*3*). While PCAF and GCN5 are typically found in large multiprotein complexes in cells such as SAGA and ADA, they exhibit robust catalytic activity as purified proteins, with high selectivity for Lys-14 in histone H3 (*4*−*7*). However, their substrate specificity in protein complexes appears to be broader, and the molecular basis for this is not understood (*1*−*3*). Dysregulation of PCAF and GCN5 (PCAF/GCN5) in genetic diseases and cancer has led to the supposition that selective inhibitors of these HATs may have therapeutic applications (*8*−*10*).

PCAF/CGN5 HAT domains belong to the GNAT superfamily which are a poorly conserved protein superfamily that includes aminoglycoside acetyltransferase antibiotic resistance enzymes and serotonin *N*-acetyltransferase, the melatonin regulatory enzyme (*11*−*13*). There are estimated to be 50−60 GNAT superfamily members in humans (*11*−*13*). These enzymes display a shared CoA binding motif and ternary complex (sequential) catalytic mechanisms, often with acetyl-CoA binding prior to the amine substrate. Acid−base catalytic residues are not absolutely conserved, but many of these enzymes appear to utilize a Tyr side chain as a hydrogen bond donor or general acid and a remote Glu or His in proton abstraction. A number of high-resolution X-ray crystal structures of different GNAT members in various liganded states are now available. Of note, GCN5 is the only superfamily member for which a ternary complex structure (histone H3 tail peptide/CoA) and a bisubstrate analogue [H3-(Me)CoA-20] complex structure (Figure 1A) have been obtained (*14*, *15*). While these two structural complexes might be expected to exhibit nearly identical features, they differ sharply in the interactions of the peptide moieties and the enzyme (Figure 1).

The histone H3 peptide in the ternary complex shows a dramatically different conformation compared with that of the peptide moiety in H3-(Me)CoA-20 in the binary complex (Figure 1C) (*14*). In fact, residues 9−13 of the histone H3 peptide appear to show more intimate interactions with residues of GCN5 than the corresponding residues of the peptide moiety from H3-(Me)CoA-20 with GCN5 (*14*, *15*).

† This work was supported by the National Institutes of Health (P.A.C., J.T.S., and F.M.) and the W. M. Keck Foundation (Y.Z.).

* To whom correspondence should be addressed. E-mail: pcole@jhmi.edu. Telephone: (410) 614-8849. Fax: (410) 614-7717.

‡ Johns Hopkins University School of Medicine.

§ Johns Hopkins University.

[1] Abbreviations: PCAF, p300/CBP accessory factor; GCN5, general control of nuclear-5; $PCAF^{Wloop}$, PCAF HAT domain containing W514Y and E641W mutations; H3-20, 20 N-terminal amino acids from histone H3 (*9*); H3-CoA-20, peptide−CoA conjugate that includes H3-20 linked through Lys-14 via an acetyl bridge to CoASH (*9*); H3-(Me)-CoA-20, peptide−CoA conjugate that includes H3-20 linked through Lys-14 via an isoproprionyl bridge to CoASH (*14*); H4-CoA-7, peptide−CoA conjugate in which the seven amino acids surrounding Lys-8 of histone H4 are linked via an acetyl bridge to CoASH (*9*).

10.1021/bi050776i CCC: $30.25
Published on Web 07/15/2005

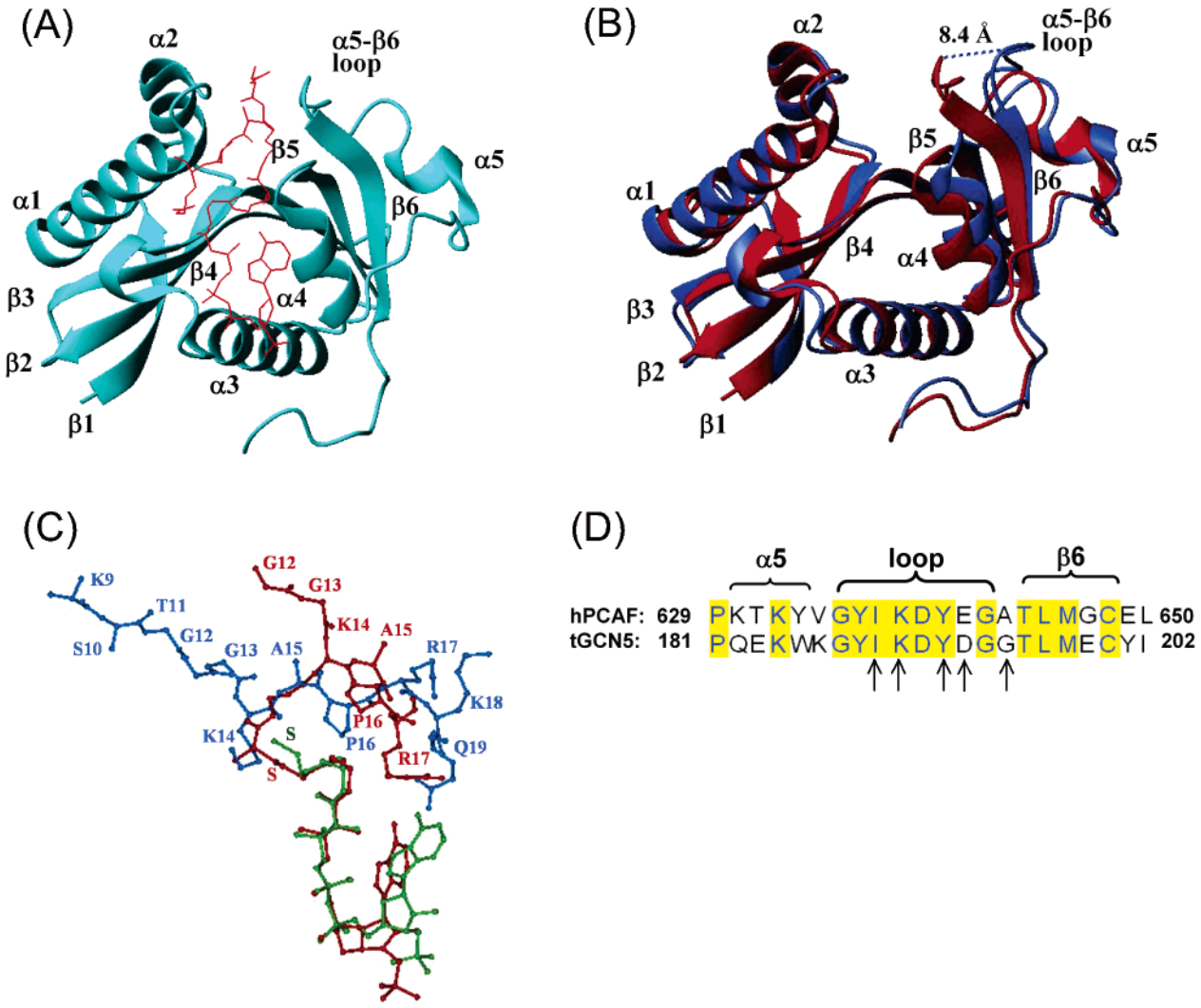

FIGURE 1: Structure of the GCN5 HAT domain in complex with the bisubstrate analogue H3-(Me)CoA-20 and comparison to the GCN5−H3-20−CoASH ternary complex (*14*). (A) X-ray structure of the GCN5−H3-(Me)CoA-20 complex with the protein colored turquoise and the bisubstrate analogue red. (B) Overlay of the protein structures of GCN5 from the ternary complex (blue) and the bisubstrate complex (red). The distance shown is that between the α-carbon of Asp-192 (corresponding to Glu-641 in PCAF) between the two conformations of the α5−β6 loop. (C) Overlay of the bisubstrate analogue (red) with the peptide substrate H3-20 (blue) and CoASH (green) from the GCN5−H3-(Me)CoA-20 complex and the ternary complex, respectively. (D) Amino acid sequences of the α5−β6 loops of PCAF and GCN5 with arrows indicating the residues mutated to tryptophan in this study. Structures were made with MOLMOL.

These more close-knit interactions with the free peptide moiety are surprising since the bisubstrate analogue H3-(Me)-CoA-20 and the desmethyl analogue H3-CoA-20 ($K_i \sim 30$ nM) exhibit binding more than 3 orders of magnitude more potent than the binding of the free peptide to PCAF/GCN5 ($K_d \sim 100$ μM) (*5*, *16*). This behavior is quite different from that of a related bisubstrate analogue peptide−nucleotide conjugate complex with a protein kinase in which the peptide moiety interactions are greater in number compared to the ternary complex (*17*).

The conformation of an enzyme loop (α5−β6) of GCN5 shows clear differences in the ternary complex versus the bisubstrate analogue complex, with the α5−β6 loop in the bisubstrate analogue complex moving ∼8 Å inward and apparently displacing the H3-CoA-20 peptide moiety (Figure 1B). Given these unexpected structural results, it has been proposed that they might result from the crystallographic conditions which are not relevant to the solution phase behavior of PCAF/GCN5. In this report, we investigate the dynamics of the human PCAF α5−β6 loop using a tryptophan fluorescence-based approach. Using site-directed mutagenesis, a residue in the α5−β6 loop (Glu-641) was identified which is catalytically tolerant toward Trp replacement, and the fluorescence properties of this Trp-substituted PCAF HAT domain have been used to investigate conformational flexibility. By employing a combination of equilibrium, rapid kinetic, and time-resolved fluorescence measurements, we have obtained evidence for loop conformational changes that are induced by bisubstrate analogue binding, validating and extending the previous crystallographic observations.

MATERIALS AND METHODS

Reagents. H3-CoA-20, H4-CoA-7, and H3-20 peptide were prepared as described previously (*9*).

Oligonucleotides were purchased from IDT. Radiolabeled agents, including [^{14}C]acetyl-CoA and [^{14}C]bovine serum albumin, were purchased from Amersham Pharmacia Biotech; CoASH was obtained from Sigma. A pET28a vector expressing the human PCAF HAT domain (amino acid residues 493−658) was obtained as described previously (*5*).

All other buffers and reagents were of the highest quality commercially available and were used without further purification.

Site-Directed Mutagenesis. All mutations were performed using the QuikChange procedure (Stratagene), confirmed by DNA sequencing, and used the following primers: W514Y, caagaagatcctgatgtatctggttggcctacag and ctgtaggccaaccagatacatcaggatcttcttg; I637W, caaatatgttggctattggaaggattatgaaggag and ctccttcataatccttccaatagccaacatatttg; K638W, caaatatgttggctatatctgggattatgaaggagccac and gtggctccttcataatcccagatatagccaacatatttg; Y640W, gttggctatatcaaggattgggaaggagccactttaatg and cattaaagtggctccttcccaatccttgatatagccaac; E641W, gctatatcaaggattattggggagccactttaatgg and ccattaaagtggctcccaataatccttgatatagc; and A643W, caaggattatgaaggatggacttaatgggatgtg and cacatcccattaaagtccatccttcataatccttg.

Protein Overexpression and Purification. Overexpression and purification of mutant PCAF HAT domain proteins was carried out in a manner analogous to that described previously (*5*). *Escherichia coli* strain BL21DE3 was used for overproduction. A frozen permanent cell line was used to inoculate 8 mL of Luria broth in Erlenmeyer flasks containing kanamycin (25 μg/mL) and allowed to grow overnight at 37 °C in a floor shaker. This culture (8 mL) was used to inoculate 1 L of Luria broth medium in flasks with kanamycin (25 μg/mL) and grown at 37 °C in a floor shaker until an OD_{595} of 0.5−0.6 was reached. The flasks were cooled by standing at 4 °C for 15 min and then induced with isopropyl 1-thio-β-D-galactopyranoside (final concentration of 0.2 mM). The culture was grown overnight in a floor shaker at 16 °C for approximately 20 h. The cells were pelleted by centrifugation (4 °C and 5000*g* for 5 min) and then resuspended in 30 mL of lysis buffer [50 mM NaHepes (pH 7.0), 500 mM NaCl, 5 mM dithiothreitol, 10% glycerol, and 1 mM phenylmethanesulfonyl fluoride]. The suspension was lysed by being passed through a French pressure cell at 15 000 psi. The insoluble protein and debris were removed by centrifugation (4 °C and 27000*g* for 30 min followed by 4 °C), and the supernatant was passed through 5 mL of chelating Sepharose resin {washed with 20 mL of water, followed by 20 mL of a 50 mM $ZnSO_4$ solution, and finally equilibrated by washing with 20 mL of equilibrium buffer [20 mM NaHepes (pH 7.0), 1 M NaCl, 30 mM imidazole, and 1 mM phenylmethanesulfonyl fluoride]} in a 60 mL column. The loaded resin was washed first with 20 mL of washing buffer A [20 mM NaHepes (pH 7.0), 1 M NaCl, 72.5 mM imidazole, and 1 mM phenylmethanesulfonyl fluoride] and then with 20 mL of washing buffer B [20 mM NaHepes (pH 7.0), 1 M NaCl, 98 mM imidazole, and 1 mM phenylmethanesulfonyl fluoride]. Fractions of 5 mL were collected as the protein was eluted off with 30 mL of elution buffer [20 mM NaHepes (pH 7.0), 1 M NaCl, 10% glycerol, 200 mM imidazole, and 100 mM EDTA]. The purified (>95%) PCAF HAT fractions (as determined by 15% SDS−PAGE stained with Coomassie) were combined and dialyzed for 2 days at 4 °C (M_r = 10 000 cutoff) against 1 L of a solution of 25 mM NaHepes (pH 7.0), 250 mM NaCl, 10 mM dithiothreitol, 1 mM EDTA, and 10% glycerol. The protein solution was concentrated by Centricon ultrafiltration and then stored at −80 °C. The final protein concentrations (1−10 mg/mL) were determined with a Bradford assay and by measuring the A_{280} in the denatured state [6 M guanidinium and 20 mM sodium phosphate (pH 6.5)] (*18*).

Acetyltransferase Assays. The radioactive HAT assay was adapted from the methods in ref *5*. The reaction buffer contained 50 mM Tris-HCl (pH 8), 1 mM DTT, 0.1 mM EDTA, and 50 μg/mL bovine serum albumin. Reactions used purified PCAF HAT enzymes at concentrations of 0.2−5 nM as needed. Assays were carried out at 30 °C with reaction volumes of 30 μL. Reactions were initiated with enzyme after the other components were equilibrated at 30 °C and quenched after 3−6 min with 6× Tris-tricine gel loading buffer. Mixtures were separated on 16% SDS Tris-tricine polyacrylamide gels and dried, and radioactivity was quantified by PhosphorImage analysis (Molecular Dynamics) by comparison to known quantities of ^{14}C-labeled bovine serum albumin standard (NEN Life Science Products). In all cases, background acetylation (in the absence of enzyme) was subtracted from the total signal. All assays were performed at least twice, and data generally agreed within 20%. Enzyme activities were demonstrated to be linear versus enzyme concentration and time in the concentration ranges that were used. Rate measurements were based on initial conditions (less than 10% consumption of the limiting substrate). In inhibition assays, the specified amounts of inhibitors were added and in all cases were at least 5-fold greater than the enzyme concentration used. For K_m(apparent) measurements, a range of a minimum of five substrate concentrations was used at fixed concentration of the second substrate (10 μM acetyl-CoA or 150 μM H3-20). The data were fitted to the Michaelis−Menten equation

$$v = V_m S/(K_m + S) \quad (1)$$

by using a nonlinear least-squares analysis (computed with KaleidaGraph). It should be noted that the PCAF acetyltransferase steady-state kinetic parameters are not greatly affected by the presence of an N-terminal His6 tag or by small changes in temperature (30 vs 25 °C) or pH (8.0 vs 7.4) (k_{cat} and K_m values within 4-fold) (*5*, *14*, *16*).

Steady-State Fluorescence Measurements. The fluorescence of PCAF^{Wloop} samples (2 mL) was measured at 25 °C in a buffer solution containing 20 mM Tris-HCl, 200 mM NaCl, 1 mM EDTA, and 10 mM DTT (pH 7.4) on a SPEX Fluoromax-2 spectrofluorometer (Instruments SA, Edison, NJ) using a 3 mL cuvette. Emission spectra were recorded over the wavelength range of 310−440 nm with an excitation wavelength of 280 nm. The slit width was 2 nm for incident light and 4 nm for emission light. In all cases, sufficient time was allowed to establish that measurements were obtained at equilibrium. The dissociation constant for H3-CoA-20 or CoASH interacting with PCAF^{Wloop} was determined by measuring fluorescence emission with increasing H3-CoA-20 or CoASH concentrations and with a fixed concentration of PCAF^{Wloop} after correcting for the inner filter effect. Since the concentration of PCAF^{Wloop} was much lower than the K_d of the PCAF−CoASH complex (see Table 1), the dissociation constant for binding of CoASH to PCAF^{Wloop} was calculated from the standard equilibrium (eq 2):

$$\text{fraction bound} = (F - F_0)/(F_f - F_0) = [L]/(K_d + [L]) \quad (2)$$

where F equals the measured fluorescence emission intensity (corrected for the inner filter effect), F_f and F_0 correspond

Table 1: Comparative Kinetic Parameters for the Wild-Type Human PCAF HAT Domain (*14*) and PCAF^{Wloop} [a]

	acetyl-CoA K_m (μM)	H3-20 K_m (μM)	k_{cat} (s^{-1})	H3-CoA-20 K_i (nM)	CoASH K_i (μM)
WT PCAF	1.6	50	3.5	124	nd[b]
PCAF^{Wloop}	2.6	19	1.8	206	21

[a] Note both of these proteins contain an N-terminal six-His tag and are identical except for mutations at Trp-514 and Glu-641. Standard errors for these values were estimated to be ±20%. [b] Not determined.

to the final and initial fluorescence emission intensities, respectively, and [L] is the CoASH concentration.

Since several H3-CoA-20 concentrations were close to the PCAF^{Wloop} concentration, the K_d of H3-CoA-20 was obtained from eq 3:

$$\text{fraction bound} = (F - F_0)/(F_f - F_0) = ({}^1/_2[\text{PCAF}]_{tot})[b - (b^2 - 4[\text{L}]_{tot}[\text{PCAF}]_{tot})^{1/2}] \quad (3)$$

$$b = K_d + [\text{L}]_{tot} + [\text{PCAF}]_{tot}$$

where F_0 and F_f are the initial and final fluorescence intensities, respectively, $[\text{PCAF}]_{tot}$ is the total PCAF^{Wloop} concentration, and $[\text{L}]_{tot}$ is the total concentration of H3-CoA-20. In the calculation, the PCAF^{Wloop} total concentration was held constant at 200 nM.

Rapid Kinetic Measurements. Stopped-flow fluorescence experiments were performed at 25 °C in the two-syringe mode using a device from Applied Photophysics (Surrey, U.K.) (dead time of 1.1 ms). A buffer solution containing 20 mM Tris-HCl, 200 mM NaCl, 1 mM EDTA, and 10 mM DTT (pH 7.4) was used for all experiments. The kinetics of H3-CoA-20 bisubstrate inhibitor association with the PCAF^{Wloop} enzyme was followed by recording the fluorescence signal enhancement over time after the rapid mixing of reactants. These experiments were carried out with 0.1 μM PCAF^{Wloop} and 0, 0.1, 0.4, 0.8, 1.6, 6.4, and 12.8 μM H3-CoA-20. The stopped-flow data were fitted to several possible mechanisms (one-step model, two-step model, and a parallel model) by nonlinear least-squares regression using *DynaFit* (*19*). This program determines, and then integrates, the system of differential equations for a given kinetic mechanism, and then uses nonlinear regression analysis to determine the best-fit parameters to the experimental data. The kinetics of dissociation of the H3-CoA-20 inhibitor from PCAF^{Wloop} was studied using irreversible conditions by following the decrease in fluorescence after rapid dilution of the complex. The dissociation was made irreversible by trapping the free H3-CoA-20 with excess nonfluorescent PCAF (W514Y), thereby preventing rebinding of the dissociated H3-CoA-20 to PCAF^{Wloop}. Although the K_i of H3-CoA-20 for PCAF W514Y has not been directly measured, its acetyltransferase activity that is similar to that of the wild-type enzyme along with the E641W, W514Y K_i measurements (Table 1) provides confidence that the high concentration (5 μM) of this mutant protein will serve as an effective trap (Table 1). Moreover, a doubling of the concentration of this mutant trap protein yielded no change in the rate constants obtained. The time course was fitted to a two-exponential decay which included a slow component with a small amplitude likely due to to photobleaching. The major component reflected the dissociation rate. In these experiments, PCAF^{Wloop} fluorescence was excited at 280 nm, and the fluorescence was monitored using a 335 nm cut-on filter.

Pico- and Nanosecond Time-Resolved Fluorescence Measurements. Time-resolved fluorescence experiments were performed at 25 °C in the buffer solution containing 20 mM Tris-HCl, 200 mM NaCl, 1 mM EDTA, and 10 mM DTT (pH 7.4). Two samples were prepared. One contained 40 μM free PCAF^{Wloop}, and the other contained 40 μM PCAF^{Wloop} and 160 μM H3-CoA-20. The samples were excited by a frequency-doubled output of a tunable picosecond dye laser described previously (*20*). The laser pulses were 11 ps wide and followed at a repetition rate of ~4.1 MHz. To minimize excitation of tyrosine residues, the exciting wavelength was tuned to 296 nm. To minimize photobleaching of tryptophan, the mean exciting power was reduced below 20 μW by a neutral density filter and the beam was defocused to a diameter of 1.5 mm before the sample was added to the sample cuvette. Fluorescence emission was passed through a magic-angle polarizer and a computer-controlled monochromator with a spectral resolution of 8 nm, and was detected by a microchannel plate photomultiplier connected to time-correlated single-photon counting electronics. The overall time resolution of the system, including the excitation laser, monochromator, photomultiplier, and electronics, was 65 ps (full width at half-maximum). Time-resolved fluorescence data were collected at 30 emission wavelengths between 305 and 450 nm. The experimental setup and the methods of data analysis have been described elsewhere (*20*).

RESULTS

Generation of PCAF^{Wloop}. The PCAF HAT domain (residues 493−658) contains a single native tryptophan (Trp-514) which is remote from the α5−β6 loop, and this residue was replaced with a Tyr residue using site-directed mutagenesis. PCAF HAT W514Y expressed and purified readily and was shown to have acetyltransferase activity within 2-fold of that of the wild type (data not shown). Next, single-Trp mutant proteins were prepared at five separate positions in the loop (637, 638, 640, 641, and 643) at the sites shown (Figure 1D). Screening of the purified double mutant proteins for acetyltransferase activity demonstrated that only two of the five loop mutants (K638W, 15% of wild-type activity; E641W, 30% of wild-type activity) had activity greater than 5% of PCAF HAT W514Y activity. The PCAF HAT mutant W514Y/E641W (PCAF^{Wloop}) was characterized in greater depth to assess its steady-state kinetic parameters [k_{cat}, K_m of acetyl-CoA, and K_m of the peptide substrate (H3-20) (*9*)] and sensitivity to inhibitors (CoASH and H3-CoA-20) (Table 1). The values for PCAF^{Wloop} appeared to be in rather good agreement with those previously determined for the WT PCAF HAT domain under similar conditions.

These results suggest that PCAF^{Wloop} should faithfully represent the catalytic behavior of the wild-type enzyme and be useful for fluorescence analysis.

Equilibrium Fluorescence Studies on PCAF^{Wloop}. Equilibrium fluorescence measurements on PCAF^{Wloop} were performed by excitation at 280 nm in the presence of different ligands. It was shown that fluorescence emission was stable with a purified enzyme concentration as low as 100 nM at room temperature and pH 7.4. By titrating increasing

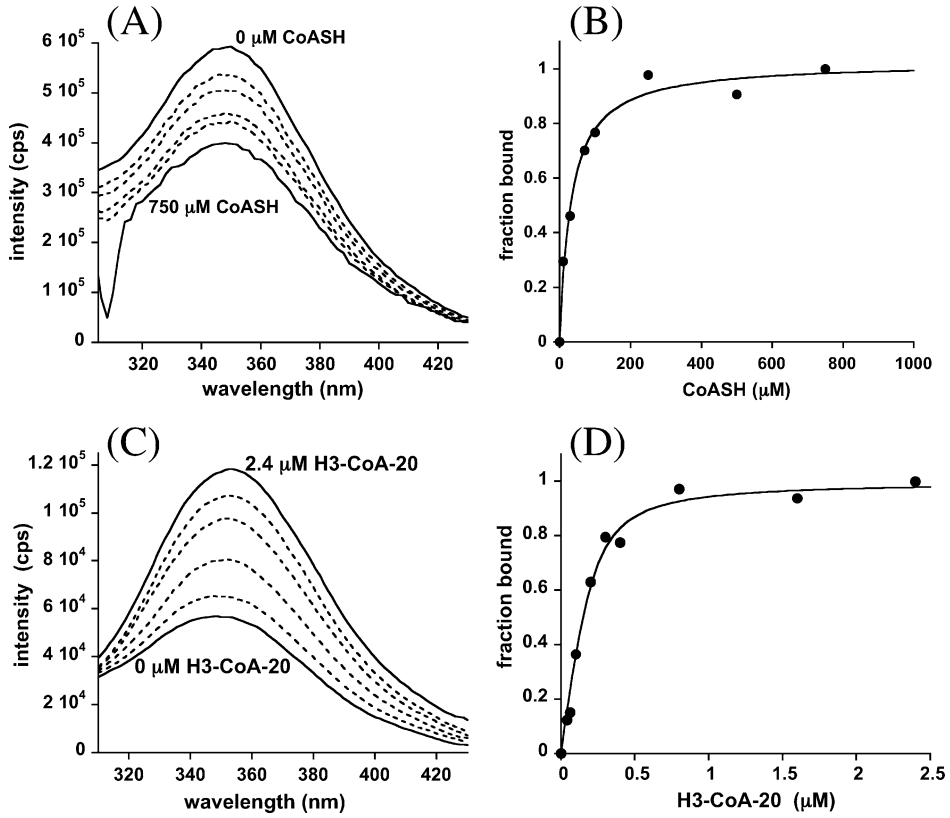

FIGURE 2: Steady-state fluorescence measurements of PCAF^{Wloop} with CoASH and H3-CoA-20. (A) Emission spectra obtained for PCAF^{Wloop} (1 μM) with increasing concentrations (0, 30, 70, 100, 250, and 750 μM) of CoASH as described in Materials and Methods. (B) Plot of the fraction bound (as a percentage of the maximal fluorescence change) vs CoASH concentration. The K_d (30 $\pm$ 2 μM) was obtained as described in Materials and Methods. (C) Emission spectra obtained for PCAF^{Wloop} (200 nM) with increasing concentrations (0, 0.04, 0.1, 0.2, 0.4, and 2.4 μM) of H3-CoA-20 as described in Materials and Methods. (D) Plot of the fraction bound (as a percentage of the maximal fluorescence change) vs H3-CoA-20 concentration. The K_d (105 $\pm$ 64 nM) was obtained as described in Materials and Methods.

concentrations of CoASH, we observed a maximum quenching of ~30% of the fluorescence emission at 347 nm, after correcting for the inner filter effect (Figure 2A). A plot of fluorescence change versus CoASH concentration showed saturable behavior with a K_d of 30 μM (Figure 2B). This K_d agreed nicely with the K_i extrapolated from steady-state kinetic analysis (Table 1).

In contrast to the fluorescence behavior with CoASH titration, PCAF^{Wloop} exhibited a dramatic 2-fold increase in fluorescence at 347 nm in the presence of saturating levels of H3-CoA-20 (Figure 2C). This fluorescence change was not seen when 50 mM H3-CoA-20 was mixed with the wild-type PCAF HAT domain (<20% reduction at maximal emission of 337 nm), nor was it observed when PCAF^{Wloop} was treated with 25 μM low-affinity [K_i > 10 μM (*9*)] bisubstrate analogue H4-CoA-7 (<10% reduction at 347 nm). Furthermore, the fluorescence increase was not observed when PCAF^{Wloop} was treated with 10 μM H3-20 peptide (*9*) by itself (<20% reduction at 347 nm) or when mixed with 0.3 mM CoASH and 0.5 mM H3-20 to simulate a ternary complex (~25% reduction in emission at 347 nm). This suggests that Trp-641 exists in a very different environment in the PCAF^{Wloop}−H3-CoA-20 complex versus that in the PCAF^{Wloop}−CoASH binary complex or the PCAF^{Wloop}−CoASH−H3-20 ternary complex. A plot of the fluorescence change versus H3-CoA-20 concentration yielded a K_d of 105 $\pm$ 64 nM (Figure 2D). The relatively large statistical error for this K_d is presumably related to the need to work at a fairly high PCAF^{Wloop} concentration because of its instability when more dilute. This value was in reasonable agreement with the K_i (206 nM) deduced from acetyltransferase inhibitory studies with PCAF^{Wloop} (Table 1).

Rapid Kinetic Analysis of the Interaction of PCAF^{Wloop} with H3-CoA-20. To examine the kinetic behavior of the fluorescence change in PCAF^{Wloop}, stopped-flow fluorescence experiments were carried out. In these studies, a fixed concentration of PCAF^{Wloop} was rapidly mixed with a second solution with varying concentrations of H3-CoA-20. As can be seen, there was a readily discernible increase in fluorescence versus time which reached a plateau within ~10 s (Figure 3A). The time taken to reach this plateau shortened with increase in H3-CoA-20 concentration (Figure 3A), indicating that the fluorescence increase was partially rate-limited by the kinetics of association of H3-CoA-20 with PCAF^{Wloop}.

Prior to the development of a kinetic model for binding of H3-CoA-20 to PCAF^{Wloop}, the dissociation of H3-CoA-20 from PCAF^{Wloop} was analyzed using a trapping experiment (Figure 3C). In this experiment, a solution of H3-CoA-20 and PCAF^{Wloop} was rapidly mixed with a second solution containing a large excess of the nonfluorescent PCAF HAT domain (W514Y). As shown, an exponential decrease in fluorescence was observed reflecting the release of H3-CoA-20 from PCAF^{Wloop}, which was followed by rapid trapping of H3-CoA-20 by the spectroscopically "invisible" PCAF HAT domain (W514Y) (Figure 3C). The dissociation rate constant for this release (0.10 $\pm$ 0.002 s^{-1}) was obtained from a fit of the data to a double-exponential decay equation,

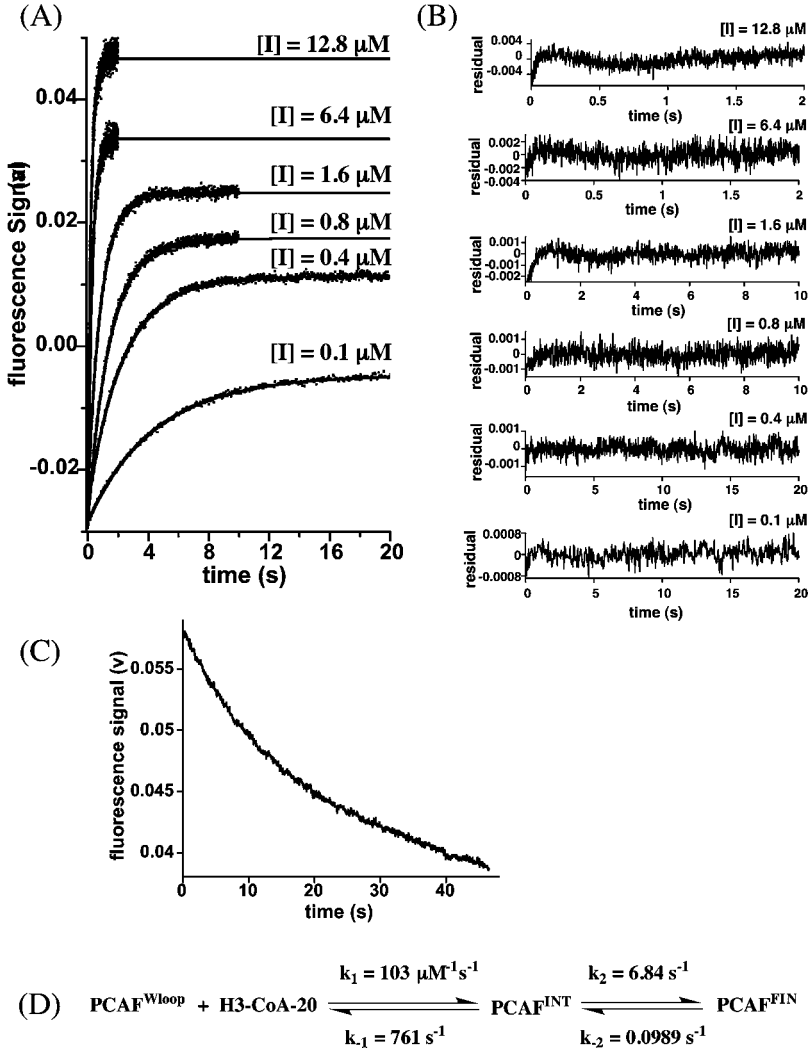

FIGURE 3: Fluorescence increase upon rapid mixing of PCAF^{Wloop} (final concentration of 0.1 μM) with H3-CoA-20 (final concentrations of 0.1, 0.4, 0.8, 1.6, 6.4, and 12.8 μM). (A) Simulated data and experimental data are superimposed. (B) Plots of the residuals from panel A. (C) Determination of the rate of dissociation of H3-CoA-20 from PCAF^{Wloop} by stopped-flow fluorescence using PCAF (W514Y) as a trap for free H3-CoA-20. A complex consisting of 0.1 μM PCAF^{Wloop} and 0.1 μM H3-CoA-20 was rapidly mixed with a solution of 5 μM PCAF HAT domain (W514Y). A k_{diss} of 0.10 $\pm$ 0.002 s^{-1} for H3-CoA-20 was measured as described in Materials and Methods. A second component (k = 0.014 $\pm$ 0.0007 s^{-1}) attributed to photobleaching was also obtained from the fit. (D) Computer-simulated model of the H3-CoA-20−PCAF interaction. The fluorescence response factors relative to PCAF^{Wloop} are 61 and 210% for PCAF^{INT} and PCAF^{FIN}, respectively. The rate constants and standard errors obtained are as follows: $k_1 = (1.03 \pm 0.2) \times 10^8$ M^{-1} s^{-1}, $k_{-1} = 761 \pm 152$ s^{-1}, $k_2 = 6.84 \pm 1.36$ s^{-1}, and $k_{-2} = 0.0989 \pm 0.0197$ s^{-1}.

in which the rapid major transient reflected dissociation of the complex and the slower minor transient (0.014 $\pm$ 0.0007 s^{-1}) was attributed to photobleaching. This 0.1 s^{-1} dissociation rate constant is in moderately good agreement with a value (0.03 s^{-1}) obtained less precisely from acetyltransferase kinetic studies under slightly different experimental conditions (*5*).

With this key kinetic constraint in hand, the data in Figure 3 were then simulated using *DynaFit* (*19*). This program allows multiple models to be tested and eliminated on the basis of visual or statistical comparisons with the observed data (see Materials and Methods). This process of elimination converged on a two-state model involving rapid association of H3-CoA-20 with PCAF^{Wloop} followed by a slow conformational change to a tightly bound form (Figure 3D). The simulations correctly predicted that the fluorescence intensity of the intermediate form (PCAF^{INT}) was ~40% lower than that of free PCAF^{Wloop}, which is similar to the fluorescence quenching observed upon equilibrium binding of CoASH to PCAF^{Wloop}. In addition, the final tightly bound form (PCAF^{FIN}) was predicted to exhibit an ~2-fold fluorescence increase compared to free PCAF^{Wloop}, which is consistent with the equilibrium binding measurements (see above). Thus, the data indicate near-diffusion-controlled association [$k_1 = (1.03 \pm 0.2) \times 10^8$ M^{-1} s^{-1}] to form a weakly bound state ($k_{-1} = 761 \pm 152$ s^{-1}), followed by a moderately rapid conformational change ($k_2 = 6.84 \pm 1.36$ s^{-1}) to from a tightly bound state ($k_{-2} = 0.0989 \pm 0.0197$ s^{-1}). The initial recognition K_i ($k_{-1}/k_1 = 7.4$ μM) is in the same range as the K_i and K_d of CoASH (30 μM). In addition, the optimized K_d obtained from the simulations ($K_d = k_{-1}k_{-2}/k_1k_2 = 107$ nM) quantitatively accounts for the observed K_d for H3-CoA-20 binding (105 $\pm$ 64 nM), as well as the acetyltransferase K_i (206 nM). Residuals for each of the binding plots are displayed in panels A and B of Figure 3 and show no large systematic differences from the measured data.

Pico- and Nanosecond Time-Resolved Tryptophan Fluorescence Measurements on PCAF^{Wloop}. Measurements of

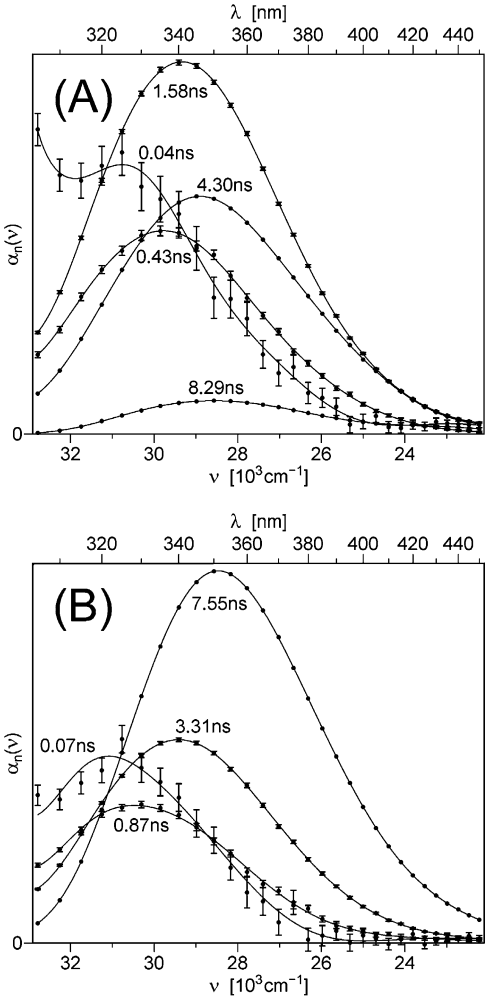

FIGURE 4: Preexponential factor spectra for free PCAF^{Wloop} (A) and its complex with H3-CoA-20 (B). The corresponding τ_n values are shown as curve labels. All spectra have been converted to the linear wavenumber (ν) scale, which also represents a linear energy scale. Circles represent the results of the global fitting. Error bars represent 95% confidence intervals (not shown for the results in which the confidence intervals are smaller than the thickness of the line). Solid lines represent polynomial interpolation; for details, see ref *20*. The concentration of H3-CoA-20 is 0 in panel A and 160 μM in panel B. The concentration of PCAF^{Wloop} is 40 μM in both cases. The exciting wavelength is 296 nm, and the temperature is 25 °C.

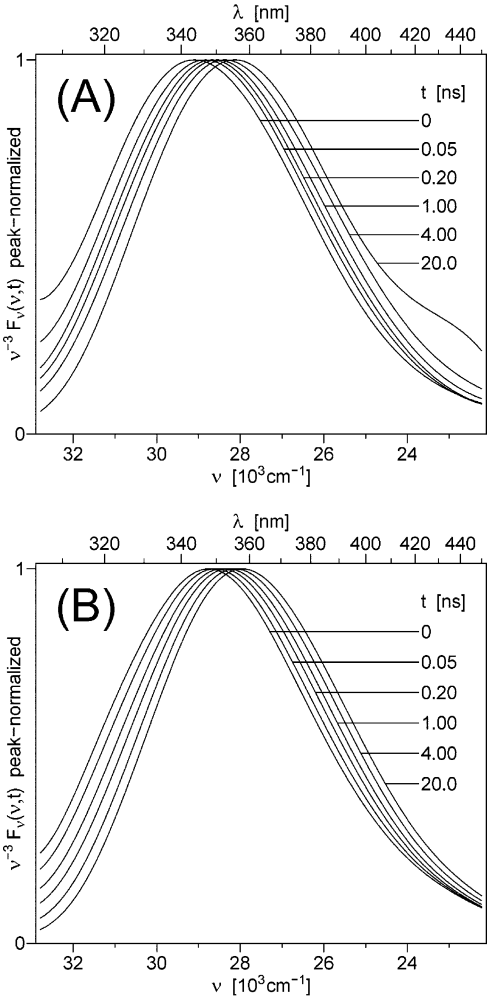

FIGURE 5: Instantaneous fluorescence emission spectra at different times after excitation for free PCAF^{Wloop} (A) and its complex with H3-CoA-20 (B). The instantaneous spectra were reconstructed from the $\alpha_n(\nu)$ spectra and τ_n values shown in Figure 4, multiplied by ν^{-3} for reasons explained previously (*20*), and peak-normalized. For experimental conditions, see the legend of Figure 4.

picosecond and nanosecond time-resolved fluorescence in proteins can provide general information about the environment surrounding the fluorescent moiety. Time-resolved measurements were made of two fluorescent samples, (A) free PCAF^{Wloop} and (B) PCAF^{Wloop} bound to H3−CoA-20; the results are shown in the corresponding panels of Figures 4 and 5. With each sample, the data were collected at 30 emission wavelengths between 305 and 450 nm and fitted globally by a linear combination of a sufficient number of exponential terms with τ_n time constants that were held equal between all emission wavelengths and α_n preexponential factors that were allowed to vary with emission wavelength:

$$I(\lambda,t) = \sum_n \alpha_n(\lambda) \exp(-t/\tau_n) \qquad (4)$$

In the case of free PCAF^{Wloop}, a minimum of five exponential terms were required for a statistically adequate fit (reduced $\chi^2 = 1.021$), whereas in the case of PCAF^{Wloop} bound to H3-CoA-20, only four exponential terms were necessary (reduced $\chi^2 = 1.012$). All $\alpha_n(\nu)$ preexponential factor spectra are depicted in Figure 4 on a linear wavenumber scale; the corresponding time constant τ_n is printed near each curve as the curve label. In the case of the PCAF^{Wloop}−H3-CoA-20 complex, the dominant exponential component corresponds to a τ of 7.55 ns, which significantly exceeds 1.58 ns, the time constant for the dominant exponential in the case of free PCAF^{Wloop}; this is consistent with the enhanced steady-state fluorescence of the complex.

Using the $\alpha_n(\nu)$ spectra and the τ_n time constants from Figure 4, we reconstructed instantaneous emission spectra at different times after excitation; the instantaneous spectra are shown in Figure 5. The decrease in the width of the instantaneous spectrum with time after excitation reveals that the ensemble of the excited fluorophores is heterogeneous, since in the case of a homogeneous ensemble the peak-normalized spectra would be identical in shape except for a parallel translation (*20*). In the case of the PCAF^{Wloop}−H3-CoA-20 complex (Figure 5B), a significant shape variation is observed only in the spectral range of <330 nm where tyrosine emission is significant; this variation can be attributed to fluorescence emission from tyrosine residues. In

the case of free PCAF^{Wloop}, significant shape variations are observed on both sides of the emission peak, which can be explained only in terms of multiple conformational states of the environment of the tryptophan group. Taken together, these results suggest that the tryptophan group in the PCAF^{Wloop}−H3-CoA-20 complex is better shielded from collisional quenching, and that its environment is confined to a narrower set of conformations than that of the tryptophan in free PCAF^{Wloop}.

DISCUSSION

Flexible loops in proteins are increasingly being shown to play important roles in the catalytic action and regulation of a variety of enzymes. Elegant studies on protein kinases (*21*, *22*), protein phosphatases (*23*), dihydrofolate reductase (*24*), triosephosphate isomerase (*25*), ketosteroid isomerase (*26*), β-lactamase (*27*), acetylcholinesterase (*28*), undecanyl pyrophosphate synthase (*29*), DNA polymerase (*30*), and galactosyltransferases (*31*) have revealed key roles for mobile loops in the functions of these enzymes. Among the biophysical tools most often employed currently in interrogating flexible loops in proteins are fluorescence, NMR, and mass spectrometry. We selected a fluorescence-based approach because of its sensitivity and because the PCAF HAT domain under investigation possessed only a single tryptophan (514) which could be readily replaced. We were fortunate in finding an $\alpha5-\beta6$ loop residue (641) within the PCAF HAT domain loop which proved to be amenable to Trp replacement, based on preservation of catalytic parameters. Because of this minimal catalytic perturbation, the fluorescent responsiveness of the PCAF^{Wloop} protein is expected to reflect mechanistically relevant information.

The rather dramatic differences between the steady-state fluorescence emission of the CoASH−PCAF^{Wloop} complex and the H3-CoA-20−PCAF^{Wloop} complex can reasonably be deduced to correspond to the two different $\alpha5-\beta6$ loop conformations previously observed in the X-ray structures of the related complexes (*14*). Thus, this solution phase optical data validate the crystallographic structures previously obtained and argue that the $\alpha5-\beta6$ loop responds dynamically to specific ligand interactions. Why the fluorescence emission intensity of PCAF^{Wloop} should increase so sharply in the presence of H3-CoA-20 cannot be answered with certainty, but two possibilities can be considered. Increased separation of Trp-641 from the neighboring Tyr-640 residue in the H3-CoA-20-bound form could reduce the proton transfer quenching effect (*32*). In a second possibility, increased rigidity of the environment of Trp-641 in the H3-CoA-20-bound form could enhance the fluorescence lifetime and increase the emission intensity by protecting the fluorophore from collisions with all possible quenchers, including the protein backbone (*33*).

It is noteworthy that studies carried out with the H3-CoA-20 bisubstrate analogue likely reflect molecular recognition characteristics of the natural substrate. The high affinity of the compound requires both the sequence and number of amino acids found to be necessary for efficient catalysis (*5*, *9*). Thus, observing a two-step binding interaction with the stopped-flow studies helps resolve the apparent paradox in which the peptide moiety seems to be relatively unimportant in the crystallized bisubstrate complex.

These studies are likely to bear directly on the PCAF/GCN5 catalytic mechanism for acetyl transfer. Since in the ternary complex, the $\alpha5-\beta6$ loop protrudes out to the surface and away from the active site, it has been proposed previously that the loop conformation in the GCN5−H3-CoA-20 structural complex may be catalytically relevant to acetyl transfer, possibly reflecting a late catalytic intermediate. Other evidence for this role came from site-directed mutagenesis studies in which mutation of Tyr-640 to Ala in PCAF was shown to greatly reduce k_{cat} but have little effect on substrate K_m values (*14*). The stopped-flow studies are consistent with the enzyme mechansim involving two kinetically distinguishable steps, binding followed by catalysis in which loop motion occurs. Kinetic analysis of the fluorescence data suggests that the $\alpha5-\beta6$ loop movement in the forward direction (k_2) occurs with a rate constant (6.84 s^{-1}) that is somewhat greater than the k_{cat} (1.8 s^{-1}) for acetyltransferase of PCAF^{Wloop}. This is consistent with the hypothesis that the $\alpha5-\beta6$ loop movement is catalytically competent to participate in acetyl transfer.

The therapeutic potential of inhibitors for PCAF/GCN5 underscores the value in detailed kinetic analysis of enzyme inhibition of lead agents such as the bisubstrate analogue H3-CoA-20. The fluorescence approach here proved to be effective in providing a more complete portrait of how this compound binds and induces a conformational change in PCAF/GCN5 which presumably leads to its high affinity. The fact that there is an apparent intermediate complex formed (PCAF^{INT}) provides a molecular explanation for why so many of the 20 residues of the peptide moiety are needed to confer potency (nine), since most of these residues appear to be disordered in the X-ray structure (*14*). It is presumably in this intermediate complex where peptide−enzyme interactions are realized on the way to the final complex. From a practical perspective, the fluorescence method developed may be applicable to high-throughput screening of inhibitors with other structural scaffolds, which may induce a related fluorescence change. This may be even more effective if the fluorophore in PCAF^{Wloop} is replaced with an unnatural fluorescent amino acid which shows less overlap with small molecule libraries. Such unnatural fluorophores could be introduced by expressed protein ligation (*34*, *35*) or biosynthetic strategies (*36*).

It is interesting to make a comparison of a flexible loop present in a different HAT enzyme, p300 (*37*), and that identified here in PCAF/GCN5. In p300, a protease sensitive loop appears to be heavily autoacetylated and serve as a regulatory module for acetyltransferase activity (*37*). Although PCAF may be regulated by autoacetylation (*38*), the loop investigated here contains only one lysine (Lys-638) which is not known to be a site of modification. Thus, it appears these different HATs are employing dynamic loops in distinct ways.

A major unanswered question in the function of PCAF/GCN5 concerns its apparently looser substrate sequence specificity in the context of multiprotein complexes (*39*). Because the $\alpha5-\beta6$ loop has the ability to dislodge interactions between peptide substrate and enzyme, it could plausibly be involved in mediating substrate specificity changes that are observed in the context of multiprotein complexes. Distinctive fluorescent probes engineered into this PCAF/GCN5 loop might allow for novel conformational insights that are induced by megacomplex formation.

ACKNOWLEDGMENT

We thank Daniel Krosky, Chunyang Cao, Ronen Marmorstein, and Cole lab members for helpful assistance and discussion.

REFERENCES

1. Roth, S. Y., Denu, J. M., and Allis, C. D. (2001) Histone acetyltransferases, *Annu. Rev. Biochem. 70*, 81−120.
2. Sterner, D. E., and Berger, S. L. (2000) Acetylation of histones and transcription-related factors, *Microbiol. Mol. Biol. Rev. 64*, 435−459.
3. Marmorstein, R. (2001) Structure of histone acetyltransferases, *J. Mol. Biol. 311*, 433−444.
4. Schiltz, R. L., Mizzen, C. A., Vassilev, A., Cook, R. G., Allis, C. D., and Nakatani, Y. (1999) Overlapping but distinct patterns of histone acetylation by the human coactivators p300 and PCAF within nucleosomal substrates, *J. Biol. Chem. 274*, 1189−1192.
5. Lau, O. D., Courtney, A. D., Vassilev, A., Marzilli, L. A., Cotter, R. J., Nakatani, Y., and Cole, P. A. (2000) p300/CBP-associated factor histone acetyltransferase processing of a peptide substrate. Kinetic analysis of the catalytic mechanism, *J. Biol. Chem. 275*, 21953−21959.
6. Grant, P. A., Duggan, L., Cote, J., Roberts, S. M., Brownell, J. E., Candau, R., Ohba, R., Owen-Hughes, T., Allis, C. D., Winston, F., Berger, S. L., and Workman, J. L. (1997) Yeast Gcn5 functions in two multisubunit complexes to acetylate nucleosomal histones: Characterization of an Ada complex and the SAGA (Spt/Ada) complex, *Genes Dev. 11*, 1640−1650.
7. Grant, P. A., Eberharter, A., John, S., Cook, R. G., Turner, B. M., and Workman, J. L. (1999) Expanded lysine acetylation specificity of Gcn5 in native complexes, *J. Biol. Chem. 274*, 5895−5900.
8. Lehrmann, H., Pritchard, L. L., and Harel-Bellan, A. (2002) Histone acetyltransferases and deacetylases in the control of cell proliferation and differentiation, *Adv. Cancer Res. 86*, 41−65.
9. Lau, O. D., Kundu, T. K., Soccio, R. E., Ait-Si-Ali, S., Khalil, E. M., Vassilev, A., Wolffe, A. P., Nakatani, Y., Roeder, R. G., and Cole, P. A. (2000) HATs off: Selective synthetic inhibitors of the histone acetyltransferases p300 and PCAF, *Mol. Cell 5*, 589−595.
10. Zheng, Y., Thompson, P. R., Cebrat, M., Wang, L., Devlin, M. K., Alani, R. M., and Cole, P. A. (2004) Selective HAT inhibitors as mechanistic tools for protein acetylation, *Methods Enzymol. 376*, 188−199.
11. Vetting, M. W., S de Carvalho, L. P., Yu, M., Hegde, S. S., Magnet, S., Roderick, S. L., and Blanchard, J. S. (2005) Structure and functions of the GNAT superfamily of acetyltransferases, *Arch. Biochem. Biophys. 433*, 212−226.
12. Zheng, W., and Cole, P. A. (2002) Serotonin *N*-acetyltransferase: Mechanism and inhibition, *Curr. Med. Chem. 9*, 1187−1199.
13. Dyda, F., Klein, D. C., and Hickman, A. B. (2000) GCN5-related *N*-acetyltransferases: S structural overview, *Annu. Rev. Biophys. Biomol. Struct. 29*, 81−103.
14. Poux, A. N., Cebrat, M., Kim, C. M., Cole, P. A., and Marmorstein, R. (2002) Structure of the GCN5 histone acetyltransferase bound to a bisubstrate inhibitor, *Proc. Natl. Acad. Sci. U.S.A. 99*, 14065−14070.
15. Rojas, J. R., Trievel, R. C., Zhou, J., Mo, Y., Li, X., Berger, S. L., Allis, C. D., and Marmorstein, R. (1999) Structure of *Tetrahymena* GCN5 bound to coenzyme A and a histone H3 peptide, *Nature 401*, 93−98.
16. Tanner, K. G., Langer, M. R., and Denu, J. M. (2000) Kinetic mechanism of human acetyltransferase, PCAF, *Biochemistry 39*, 11961−11969.
17. Parang, K., Till, J. H., Ablooglu, A. J., Kohanski, R. A., Hubbard, S. R., and Cole, P. A. (2001) Mechanism-based design of a protein kinase inhibitor, *Nat. Struct. Biol. 8*, 37−41.
18. Gill, S. C., and von Hippel, P. H. (1989) Calculation of protein extinction coefficients from amino acid sequence data, *Anal. Biochem. 182*, 319−326.
19. Kuzmic, P. (1996) Program DYNAFIT for the analysis of enzyme kinetic data: Application to HIV proteinase, *Anal. Biochem. 237*, 260−273.
20. Toptygin, D., Savtchenko, R. S., Meadow, N. D., and Brand, L. (2001) Homogeneous spectrally- and time-resolved fluorescence emission from single-tryptophan mutants of IIA(Glc) protein, *J. Phys. Chem. B 105*, 2043−2055.
21. Adams, J. A. (2003) Activation loop phosphorylation and catalysis in protein kinases: Is there functional evidence for the autoinhibitor model? *Biochemistry 42*, 601−607.
22. Huse, M., and Kuriyan, J. (2002) The conformational plasticity of protein kinases, *Cell 109*, 275−282.
23. Juszczak, L. J., Zhang, Z. Y., Wu, L., Gottfried, D. S., and Eads, D. D. (1997) Rapid loop dynamics of *Yersinia* protein tyrosine phosphatases, *Biochemistry 36*, 2227−2236.
24. Venkitakrishnan, R. P., Zaborowski, E., McElheny, D., Benkovic, S. J., Dyson, H. J., and Wright, P. E. (2004) Conformational changes in the active site loops of dihydrofolate reductase during the catalytic cycle, *Biochemistry 43*, 16046−16055.
25. Parthasarathy, S., Eaazhisai, K., Balaram, H., Balaram, P., and Murthy, M. R. (2003) Structure of *Plasmodium falciparum* triosephosphate isomerase-2-phosphoglycerate complex at 1.1-angstrom resolution, *J. Biol. Chem. 278*, 52461−52470.
26. Nam, G. H., Cha, S. S., Yun, Y. S., Oh, Y. H., Hong, B. H., Lee, H. S., and Choi, K. Y. (2003) The conserved cis-Pro(39) residue plays a crucial role in the proper positioning of the catalytic base Asp(38) in ketosteroid isomerase from *Comamonas testosteroni*, *Biochem. J. 375*, 297−305.
27. Garrity, J. D., Pauff, J. M., and Crowder, M. W. (2004) Probing the dynamics of a mobile loop above the active site of L1, a metallo-β-lactamase from *Stenotrophomonas maltophilia*, via site-directed mutagenesis and stopped-flow fluorescence spectroscopy, *J. Biol. Chem. 279*, 39663−39670.
28. Boyd, A. E., Dunlop, C. S., Wong, L., Radic, Z., Taylor, P., and Johnson, D. A. (2004) Nanosecond dynamics of acetylcholinesterase near the active center gorge, *J. Biol. Chem. 279*, 26612−26618.
29. Chang, S. Y., Chen, Y. K., Wang, A. H., and Liang, P. H. (2003) Identification of the active conformation and the importance of length of the flexible loop 72−83 in regulating the conformational change of undecaprenyl pyrophosphate synthase, *Biochemistry 42*, 14452−14459.
30. Dalal, S., Kosa, J. L., and Sweasy, J. B. (2004) The D246V mutant of DNA polymerase β misincorporates nucleotides: Evidence for a role for the flexible loop in DNA positioning within the active site, *J. Biol. Chem. 279*, 577−584.
31. Ramakrishnan, B., Boeggeman, E., and Qasba, P. K. (2004) Effect of the Met344His mutation on the conformational dynamics of bovine β-1,4-galactosyltransferase: Crystal structure of the Met344His mutant in complex with chitobiose, *Biochemistry 43*, 12513−12522.
32. Chen, Y., and Barkley, M. D. (1998) Toward understanding tryptophan fluorescence in proteins, *Biochemistry 37*, 9976−9982.
33. Callis, P. R., and Vivian, J. T. (2003) Understanding the variable fluorescence quantum yield of tryptophan in proteins using QM-MM simulations. Quenching by charge transfer to the peptide backbone, *Chem. Phys. Lett. 369*, 409−414.
34. Muir, T. W., Sondhi, D., and Cole, P. A. (1998) Expressed protein ligation: A general method for protein engineering, *Proc. Natl. Acad. Sci. U.S.A. 95*, 6705−6710.
35. Evans, T. C., Jr., Benner, J., and Xu, M. Q. (1998) Semisynthesis of cytotoxic proteins using a modified protein splicing element, *Protein Sci. 7*, 2256−2264.
36. Wang, L., and Schultz, P. G. (2004) Expanding the genetic code, *Angew. Chem., Int. Ed. 44*, 34−66.
37. Thompson, P. R., Wang, D., Wang, L., Fulco, M., Pediconi, N., Zhang, D., An, W., Ge, Q., Roeder, R. G., Wong, J., Levrero, M., Sartorelli, V., Cotter, R. J., and Cole, P. A. (2004) Regulation of the p300 HAT domain via a novel activation loop, *Nat. Struct. Mol. Biol. 11*, 308−315.
38. Santos-Rosa, H., Valls, E., Kouzarides, T., and Martinez-Balbas, M. (2003) Mechanisms of P/CAF auto-acetylation, *Nucleic Acids Res. 31*, 4285−4292.
39. Poux, A. N., and Marmorstein, R. (2003) Molecular basis for Gcn5/PCAF histone acetyltransferase selectivity for histone and nonhistone substrates, *Biochemistry 42*, 14366−14374.

BI050776I